ISSN: 2710-0588

Numerical Simulation of Seismic Performance of Ultra High Performance Concrete Columns

Dongyang Zhou

School of civil engineering, Henan Polytechnic University, Jiaozuo 454000, Henan, China

Abstract

In order to study the seismic performance of ultra-high-performance concrete (UHPC) columns, ABAQUS finite element software was used to simulate the seismic performance tests of UHPC columns under horizontal loads. The simulation results were compared with existing experimental results, showing good agreement. Based on this, the hysteresis curves and skeleton curves of UHPC columns under different parameters were studied using the variable control method to investigate the effects of axial compression ratio, stirrup spacing, and longitudinal reinforcement ratio on the seismic performance of UHPC columns. The results show that with the increase of the axial compression ratio, the bearing capacity of UHPC columns is significantly improved. However, the area of the hysteresis curve decreases with increasing axial compression ratio, ductility is reduced, failure mode tends to become brittle, and seismic performance decreases as the axial compression ratio increases. Changes in stirrup spacing and longitudinal reinforcement ratio can both improve the seismic performance of UHPC columns.

Keywords

Ultra-high Performance Concrete, Seismic Performance, Low-cycle Repeated Loading, Numerical Simulation.

1. Introduction

Ultra-High Performance Concrete (UHPC) is a novel cementitious engineering material. It contains no coarse aggregates and achieves optimized gradation through the addition of fine particles such as silica fume and fly ash. The incorporation of high-efficiency water-reducing agents and steel fibers enhances the concrete's durability and suppresses crack propagation,thereby yielding outstanding mechanical properties[1-3]. Compared to ordinary concrete, UHPC possesses extremely high compressive strength, superior flexural strength, excellent plasticity and ductility, as well as outstanding durability[4]. Given the outstanding mechanical properties of UHPC, its application in structural engineering within earthquake-prone regions can significantly enhance the seismic resistance of building structures and extend their service life. Extensive experimental research on the seismic performance of UHPC columns has been conducted by scholars both domestically and internationally. Ma Fudong[5] investigated the seismic performance of beam-column joints reinforced with UHPC in the core zone. When the UHPC content was high, the damage resistance of the core zone stirrups was significantly enhanced, and UHPC substantially improved the seismic capacity of beam-column structures. Ju Yanzhong[6,7] conducted experimental studies on the seismic performance of UHPC columns and performed numerical simulations using ABAQUS finite element software. The results indicate that factors such as steel fiber content, axial compression ratio,reinforcement ratio and stirrup ratio significantly influence the seismic performance of UHPC columns. Zhao Guanyuan[8] conducted quasi-static tests on four small-scale UHPC rectangular columns to investigate the ductility performance,hysteretic curves, and failure

ISSN: 2710-0588

mechanisms of reinforced UHPC columns. They analyzed the influence of stirrup ratio on the ductility of reinforced UHPC columns.

With the continuous advancement of computer technology, finite element-based numerical simulation methods have become a viable technique for studying the seismic performance of UHPC columns.Therefore, this paper employs ABAQUS finite element software to conduct seismic analysis on UHPC columns, establishing a finite element model of the UHPC column and performing parameter analysis. After validating the rationality of the UHPC column model, this study further investigates the effects of axial compression ratio, longitudinal reinforcement ratio, and stirrup spacing on the seismic performance of UHPC columns. This research provides a reference for the application of UHPC columns in seismic engineering

2. Establishment of the Finite Element Model

2.1. Test Overview

Based on the seismic performance tests of UHPC columns in Reference[9], a finite element model of the UHPC column was established using ABAQUS finite element software. The cross-sectional dimensions of the UHPC column specimen were 250mm×250mm, with a net height of 1200mm, a foundation height of 450mm, and a concrete cover thickness of 20mm. The longitudinal reinforcement consisted of high-strength steel bars with a yield strength of 630MPa, while the stirrups were made of HRB400 steel bars. The specific parameters of the UHPC test column are shown in Table 1. The UHPC column consists of the column body, base, and reinforcement cage. Wing plates were added during testing to facilitate the application of horizontal forces to the UHPC column. In numerical simulations, vertical loads and horizontal displacements can be directly applied at the column top. Therefore, the wing plates used to fix the column during horizontal loading tests were removed from the finite element model, as shown in Fig. 1. Point RP in the figure represents the loading point for applying axial pressure and horizontal load. The UHPC column model established in ABAQUS finite element analysis employs reduced-integration eight-node linear hexahedral elements (C3D8R elements), while reinforcement is simulated using two-node linear three-dimensional truss elements (T3D2 elements).

Table 1. Specimen Parameters

Specimen Number	Longitudinal reinforcement configuration	Longitudinal reinforcement ratio	Stirrup Configuration	Stirrup reinforcement ratio	Axial compression ratio
UC3	4E18	1.62%	C10@100	1.74%	0.10
UC4	4E22	2.43%	C10@100	1.74%	0.15
UC6	4E18	1.62%	C10@100	1.74%	0.15

Note: C and E denote HRB400 and high-strength steel bars with a yield strength of 630 MPa, respectively.

ISSN: 2710-0588

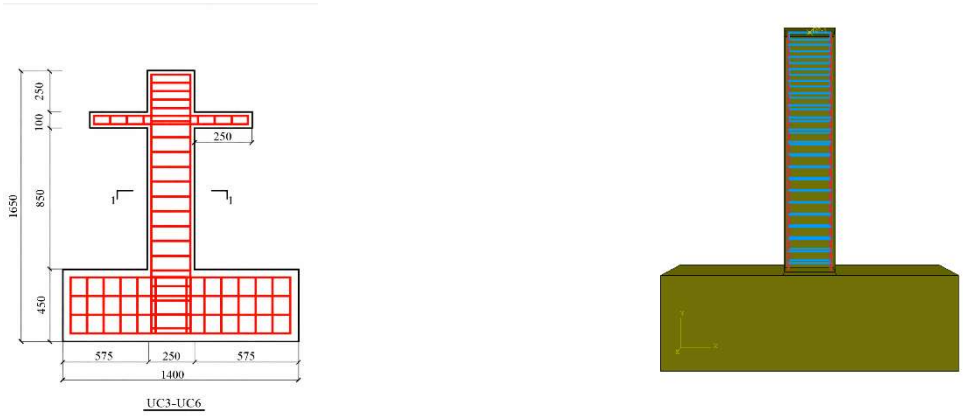

Front View of Test Specimen Finite Element Specimen Model

Fig. 1 Specimen Model and Finite Element Model

2.2. Compressive Stress-Strain Relationship of Concrete

The UHPC stress-strain relationship under compression selected in this paper was derived through inductive analysis based on a comprehensive review of domestic and international UHPC axial compression test data. Its specific expression is shown in Equation 1.

$$\sigma_c = \begin{cases} E_0\varepsilon_c\left[\dfrac{E_0}{E_s}-\left(\dfrac{E_0}{E_s}-1\right)\left(1+\dfrac{E_s}{E_0}\right)^{\frac{\varepsilon_c}{\varepsilon_{c0}}}\right] \left(0\le\varepsilon_c\le\varepsilon_{c0}\right) \\ \dfrac{\sigma_{c0}\left(\dfrac{\varepsilon_c}{\varepsilon_{c0}}\right)^{\alpha}}{1+5.09\left(\varepsilon_c-\varepsilon_{c0}\right)}\left(\varepsilon_c\ge\varepsilon_{c0}\right) \end{cases} \tag{1}$$

$$E_0 = \frac{10^3}{13.95+\dfrac{1258.17}{f_{cu}}}$$
$$\varepsilon_0 = \left(0.2f_{cu}+8.155\right)\times10^{-4} \tag{2}$$

In the equation, σc and εc represent the stress and strain of concrete under compression, while σc0 and εc0 denote the peak compressive stress and peak compressive strain. E_0 is the initial elastic modulus, and is the compressive secant modulus, which is the ratio of peak compressive stress to peak compressive strain and can be calculated using Equation 2. The value of α is related to the compressive strength (fcu) of the UHPC cube, where α = -0.00864fcu + 0.1388. The specific values for the compressive strength, elastic modulus, peak compressive stress, and peak compressive strain of the UHPC cube are shown in Table 2.

2.3. Tensile Stress-Strain Relationship of Concrete

This study examines the tensile stress-strain relationship of ultra-high performance concrete (UHPC), investigating the influence of steel fiber content on its tensile strength and deformation properties. The tensile constitutive relationship for UHPC proposed by Yang Zhihui[10] is adopted, with the specific expression given in Equation 3. The peak tensile stress and peak tensile strain of UHPC are presented in Table 2.

ISSN: 2710-0588

$$y=\begin{cases} Ax+(3-2A)x^2+(A-2)x^3 \ (0\le x\le 1) \\ \dfrac{x}{\lambda(x-1)^{\beta}+x}(x\ge 1) \end{cases} \tag{3}$$

In the equation, x=εt/εt0, y=σt/σt0, where εt and σt represent the strain and stress of UHPC under tension, respectively; εt0 denotes the peak strain of UHPC under tension, and σt0 denotes the peak stress under tension. A represents the rising-phase parameter, while λ is the falling-phase parameter related to the volume fraction of steel fibers. Based on the 2% volume fraction of steel fibers in the UHPC column specimens reported in Reference 9, A is set to 1.106, λ to 5, and β to 1.7.

Table 2. UHPC Material Parameters

Compressive Strength of Cubes /Mpa	Poisson ratio	Modulus of elasticity /Mpa	Peak stress under compression /Mpa	Peak Strain Under Compression	Peak tensile stress /Mpa	Peak tensile strain
117.3	0.2	40525	104.63	0.003162	10.76	0.000337

2.4. Determination of Concrete Damage Factors

ABAQUS finite element software provides three concrete constitutive models to simulate the mechanical behavior of concrete under stress conditions, including the plastic damage model (abbreviated as CDP model). This model assumes concrete to be an isotropic material to simulate its non-elastic behavior under loading, effectively modeling the stress state of concrete under arbitrary loads with high convergence[11]. When simulating concrete using ABAQUS finite element software, damage factors must be input to model the damage progression in UHPC columns under repeated loading. This ensures numerical simulations better align with experimental processes, thereby enhancing the accuracy of UHPC column simulations.

Sidoroff's principle of energy equivalence states that the elastic residual energy generated by stress acting on damaged materials is formally identical to that generated on undamaged materials. This equivalence is achieved by substituting equivalent stress for actual stress and replacing the elastic modulus with the elastic modulus at the point of material damage[12].

$$\sigma=E_0(1-d)^2\varepsilon \tag{4}$$

By incorporating the stress-strain relationship of UHPC, the damage factor calculation formula can be derived.

$$\begin{aligned} d_c&=1-\sqrt{\left[\frac{E_0}{E_s}-\left(\frac{E_0}{E_s}-1\right)\left(\frac{E_s}{E_0}+1\right)^{\frac{\varepsilon_c}{\varepsilon_{c0}}}\right]}(0\le\varepsilon_c\le\varepsilon_{c0}) \\ d_c&=1-\sqrt{\frac{\sigma_{c0}\left(\dfrac{\varepsilon_c}{\varepsilon_{c0}}\right)^{\alpha}}{E_0\varepsilon_c\left[1+5.09(\varepsilon_c-\varepsilon_{c0})\right]}}(\varepsilon_c\ge\varepsilon_{c0}) \end{aligned} \tag{5}$$

Similarly, the formula for the tensile damage factor can be derived.

ISSN: 2710-0588

$$d_t = 1 - \sqrt{\frac{\sigma_{t0}}{E_0 \varepsilon_{t0}}\left(1.106 + 0.788x - 0.894x^2\right)} \left(0 \le x \le 1\right)$$
$$d_t = 1 - \sqrt{\frac{\sigma_{t0}}{E_0 \varepsilon_{t0}\left[5\left(x-1\right)^{1.7} + x\right]}} \left(x \ge 1\right) \quad (6)$$

When simulating the mechanical properties of concrete under loading conditions using the CDP model in ABAQUS, it is necessary to input the relationship between the compression damage factor dc and the compression inelastic strain ε~in, as well as the relationship between the tension damage factor dt and the cracking strain ε~ck. The compression and tension damage factors can be calculated using the aforementioned formula. The compression inelastic strain and tension strain can be derived from Equation 7 based on their definitions in ABAQUS software.

$$\varepsilon_c^{\sim in} = \varepsilon_c - \frac{\sigma_c}{E_0}$$
$$\varepsilon_t^{\sim ck} = \varepsilon_t - \frac{\varepsilon_t}{E_0} \quad (7)$$

The relationship between concrete damage factors and inelastic strain is shown in Fig. 2:

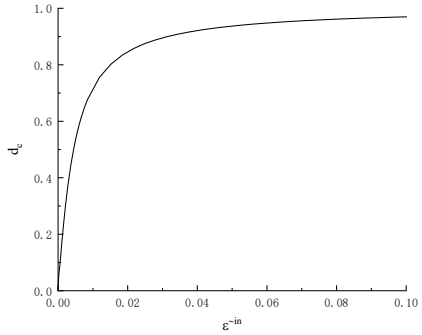

(a) Relationship between Compressive Damage Factors and Compressive Inelastic Strain

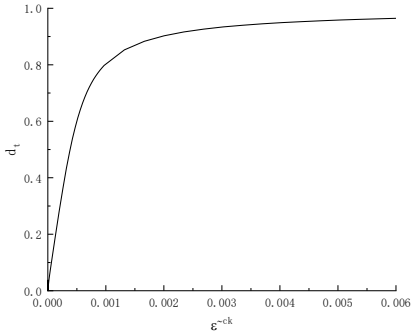

(b) Relationship between tensile damage factors and tensile inelastic strain

Fig.2 Relationship between damage factor and inelastic strain

2.5. Concrete Reinforcement Constitutive Model

The reinforcement constitutive model selected in this paper is a stress-strain hysteresis curve for reinforced concrete structures proposed by Fang Zihu[13]. This model consists of an envelope curve for the stress-strain relationship under monotonic loading and a cyclic path. Monotonic loading employs a double-break nonlinear constitutive relationship, while reloading utilizes a cubic curve, as shown in Fig. 3. During the monotonic loading phase, the reinforcing steel initially behaves in a linear elastic state, where stress and strain exhibit a linear relationship. Once stress reaches the yield strength, the steel enters a plastic development stage, where stress increases with strain at a smaller rate of strengthening stiffness. This phase demonstrates the steel's excellent ductility and deformation capacity. Under repeated loading conditions, the hysteretic behavior of reinforcing bars is significantly influenced by historical deformation. During the unloading phase, a linear unloading path is adopted, with stiffness

ISSN: 2710-0588

progressively decreasing as cyclic deformation develops. This reflects the cumulative plastic deformation of the bars and the detrimental effect of deteriorating bond properties between steel and concrete on stiffness. As unloading proceeds, the zero-stress point gradually shifts, and residual deformation continuously accumulates. During the reloading phase, the reinforcement initially exhibits pronounced low stiffness characteristics with slow stress growth, and the hysteresis curve shows contraction near zero stress. As deformation continues to develop, the reinforcement gradually recovers its collaborative load-bearing capacity with the concrete, with stiffness progressively increasing and ultimately approaching the envelope curve of monotonic loading. By incorporating a hysteretic energy dissipation coefficient, the model accurately depicts the gradual degradation of energy dissipation capacity in steel bars under cyclic loading. This realistically reproduces the pinching-type hysteretic behavior commonly observed in reinforced concrete members subjected to seismic forces.

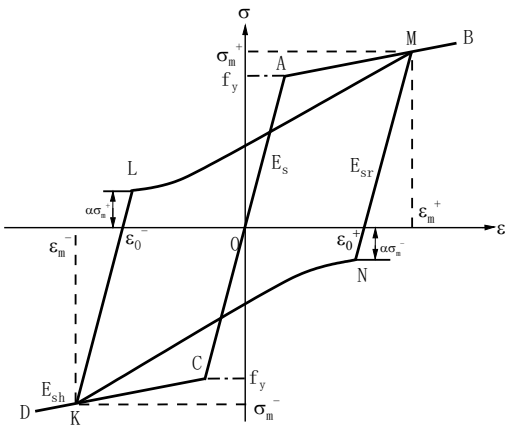

Fig.3 Reinforcement Constitutive Model

The MN and KL segments represent the unloading phase, while the LM and NK segments representthe reloading phase. Points M and K represent the points of maximum tensile stress and maximum compressive stress strain for the reinforcement. σm+ and σm- denote the maximum tensile stress andmaximum compressive stress, respectively. εm+ and εm- denote the maximum tensile strain and maximum compressive strain, respectively. ε0+ and ε0- represent the strain values where the tensile-compression unloading segment intersects the strain coordinate axis. α represents the hysteretic energy dissipation coefficient. Esc denotes the initial stiffness of the reinforcement, Esh represents the hardening stiffness, and Esr denotes the unloading stiffness. Here, β=(εm-ε0)/εy. The model loading path formulais given by Equation 8.

$$\sigma = \rho\left(\bar{\varepsilon}^{3} - \bar{\varepsilon}^{2}\right) + \left(1-\alpha\right)\sigma_m \bar{\varepsilon} + \alpha\sigma_m \tag{8}$$

In the equation, ρ=Esh(σm-σL)-(1-α)σm, ε=(ε-εL)/(εm-εL) where εL is the strain at point L or N in Figure 3. The unloading stiffness Esr and hysteresis energy dissipation coefficient α vary with changes in β.

ISSN: 2710-0588

$$E_{sr}=\begin{cases}E_s\left(\beta<1\right)\\(1.05-0.05\beta)E_s\left(1\le\beta\le4\right)\\0.85E_S\left(\beta>4\right)\end{cases}$$
$$\alpha=\begin{cases}0.5(\beta\le1)\\(20-\beta)/38(1<\beta<20)\\0(\beta\ge20)\end{cases} \quad (9)$$

2.6. Boundary Conditions and Loading Methods

The model employs column-end loading, establishing a reference point at the top of the column to apply loads. This reference point is coupled to the column top surface, while the foundation base remains fully fixed. Vertical loads in the y-direction and horizontal loads in the x-direction are applied at the reference point. The horizontal loads are applied using displacement control loading, divided into two stages. Phase 1: The displacement angles corresponding to the displacement amplitudes applied per cycle are 0.1%, 0.2%, 0.4%, 0.6%, 0.8%, and 1.0%, with only one cycle performed per load application. Phase 2: The displacement angles corresponding to the displacement amplitudes applied per cycle are 1.0%, 2.0%, 3.0%, and 4.0%, with three cycles performed per load application. As shown in Fig. 4.

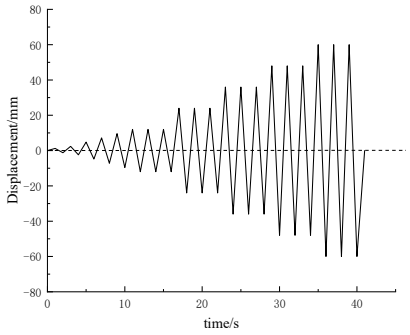

Fig. 4 Loading Method

3. Numerical Simulation Analysis

Finite element analysis was conducted on three UHPC columns with different stirrup ratios and axial compression ratios from Reference 9. The simulation results were compared with experimental data. Upon completion of the simulation, load and displacement data at the loading points of the UHPC columns were extracted via ABAQUS field variables and plotted as hysteresis curves. The skeleton curve of the UHPC columns was obtained by connecting the outermost peak points of each hysteresis loop in the hysteresis curves.

3.1. Hysteresis Curve Comparison

The comparison between the experimental hysteresis curve of the UHPC column and the simulated hysteresis curve is shown in Fig. 5. It can be observed that the experimental hysteresis curve of the UHPC column closely matches the simulated hysteresis curve during the initial loading stage. This indicates that the finite element simulation can accurately reproduce the mechanical behavior of the UHPC column during the initial loading process. As displacement increases, noticeable discrepancies emerge between the experimental and simulated hysteresis curves during the late stages of both forward and reverse loading. This may stem from differences between the bond slip between steel and concrete simulated in the finite element model and actual conditions. Overall, the experimental hysteresis curve of the

ISSN: 2710-0588

UHPC column remains fundamentally consistent with the simulated curve, demonstrating good agreement.

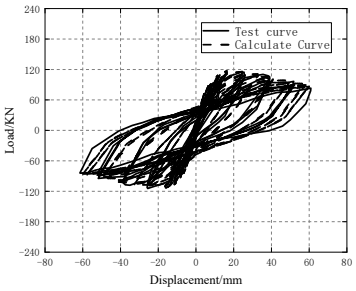

UC3 Hysteresis Curve Comparison

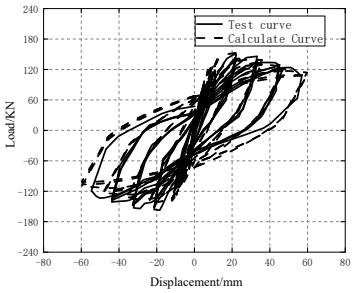

UC4 Hysteresis Curve Comparison

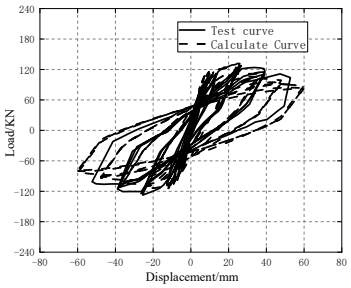

UC6 Hysteresis Curve Comparison

Fig. 5 Comparison of Hysteresis Curves

3.2. Skeleton Curve Comparison

The comparison of skeleton curves extracted from hysteresis loops of test results and simulation results for high-strength steel-reinforced UHPC columns is shown in Figure 6. It can be observed that the ascending segments of skeleton curves for all three UHPC column specimens under horizontal cyclic loading were well simulated, with computational curves exhibiting the same trend as experimental curves. However, after reaching the peak point, the simulated skeleton curve deviates from the experimental skeleton curve. This discrepancy may stem from insufficiently accurate consideration of bond slip between reinforcement and concrete in the simulation, which overlooks the influence of complex microstructures and loading forces on material behavior.

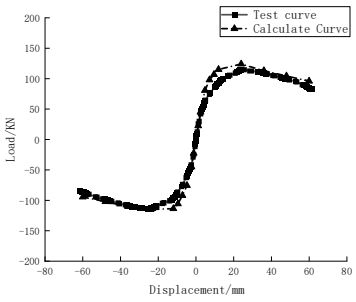

UC3 Skeletal Curve Comparison

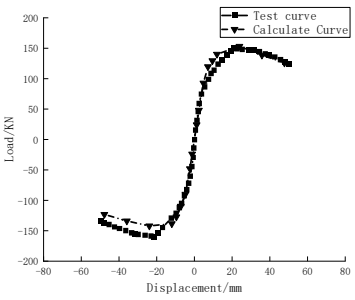

UC4 Skeletal Curve Comparison

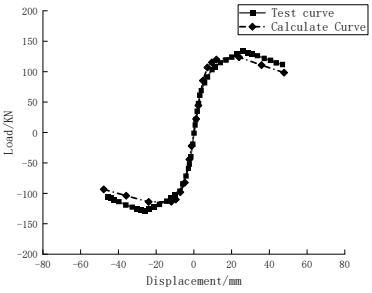

UC6 Skeletal Curve Comparison

Fig. 6 Comparison of Skeleton Curves

The results of the skeletal curve simulation analysis compared with experimental data are shown in Table 3. The comparison reveals that the peak load of the simulated skeletal curve for the UHPC column under positive loading exhibits a smaller error compared to the test data. However, the simulated peak load under reverse loading shows a slightly larger error relative to the test data. The peak displacement also exhibits some error, which may be attributed to the omission of complex factors such as micro-defects within the concrete material, crack propagation, and interfacial effects. Overall, the skeletal curves from UHPC column experiments and simulations exhibit consistent trends, with simulation results showing good agreement with experimental data. Therefore, the UHPC column model established using ABAQUS finite

ISSN: 2710-0588

element software in this study is suitable for conducting numerical analysis of seismic performance.

Table 3. Comparison of Experimental and Simulated Values

Specimen Number	Loading Direction	Peak load			Peak displacement		
		Test value /KN	Simulated value /KN	error /%	Test value /mm	Simulated value /mm	error /%
UC3	forward	116.00	124.02	6.47	24.13	23.96	0.70
	backward	-113.85	-115.01	1.01	-25.65	-23.96	6.59
UC4	forward	151.03	153.17	1.40	20.53	23.88	14.03
	backward	-158.49	-142.03	10.39	-21.62	-23.88	9.46
UC6	forward	133.96	123.80	7.58	25.80	23.91	7.33
	backward	-127.93	-114.09	10.82	-26.09	-23.91	8.36

4. Analysis of Parameters Affecting Seismic Performance

To further investigate the influence of seismic performance on UHPC columns under quasi-static loading, a variable parameter analysis was conducted based on the UC3 specimen. This study examined the effects of parameters such as axial compression ratio, longitudinal reinforcement ratio, and stirrup spacing on the seismic performance of UHPC columns. The finite element model parameters, simulation results, hysteresis curve, and characteristic data points of the skeleton curve are presented in Table 4. The deformation capacity of the specimens was evaluated using the ratio of ultimate displacement to yield displacement, termed the displacement ductility coefficient.

Table 4. Design Parameters and Simulation Results

Specimen Number	Longitudinal reinforcement ratio /%	Stirrup reinforcement ratio /%	Axial compression ratio	Loading Direction	Yield load /Mpa	Yield displacement /mm	Ultimate Load /Mpa	Maximum displacement /mm	Displacement Ductility Coefficient
ZZY1	1.62	1.74	0.1	forward	107.69	9.82	105.42	45.14	4.59
				backward	99.32	8.44	97.76	54.9	6.50
ZZY2	1.62	1.74	0.2	forward	115.81	7.59	106.40	34.97	4.60
				backward	102.78	7.47	99.99	-32.58	4.36
ZZY3	1.62	1.74	0.3	forward	130.81	8.41	119.15	22.82	2.71
				backward	116.02	6.92	101.86	19.98	2.89
ZZJ1	1.29	1.74	0.1	forward	98.29	8.98	95.27	47.93	5.33
				backward	89.32	7.65	88.15	47.93	6.26
ZZJ2	2.01	1.74	0.1	forward	118.95	10.68	116.71	48.46	4.54
				backward	112.48	9.37	108.88	59.11	6.30
ZZJ3	2.43	1.74	0.1	forward	131.97	11.41	128.62	51.69	4.53
				backward	126.41	10.40	121.73	59.48	5.72
ZGJ1	1.62	2.90	0.1	forward	107.48	10.00	105.62	57.86	5.79
				backward	101.70	9.11	99.95	56.35	6.18
ZGJ2	1.62	2.18	0.1	forward	110.60	10.23	108.17	41.07	4.01
				backward	100.07	8.61	99.82	49.76	5.78
ZGJ3	1.62	1.45	0.1	forward	105.31	9.46	103.29	46.29	4.89
				backward	97.11	8.29	96.60	48.95	5.90

4.1. Axial Compression Ratio

Fig. 7 shows the hysteresis curves and skeleton curves of UHPC columns at different axial compression ratios of 0.1, 0.2, and 0.3. During the initial loading stage, all specimens exhibit a distinct elastic phase. However, as specimens enter the yield stage, higher axial compression ratios result in greater stiffness and increased load-bearing capacity. Yet, specimens also yield earlier. After reaching peak load, specimens with higher axial compression ratios experience accelerated stiffness degradation, with stiffer specimens exhibiting steeper declines in the descending phase of the skeleton curve. causing rapid load decline and reduced ductility. When the axial compression ratio increases to a certain level, UHPC column members exhibit pronounced brittle behavior.

ISSN: 2710-0588

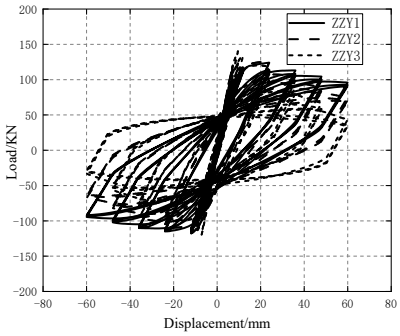

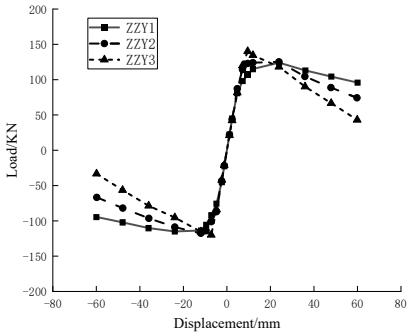

Hysteresis Curve Comparison Skeleton Curve Comparison

Fig. 7 Comparison of Axial Compression Ratios of UHPC Columns

4.2. Longitudinal Reinforcement Ratio

Fig. 8 shows the hysteresis curves and extracted skeleton curves for UHPC columns at different longitudinal reinforcement ratios. It is evident that the hysteresis curves and extracted skeleton curves of UHPC columns exhibit essentially identical shapes. As the longitudinal reinforcement ratio increases, the peak load and ultimate load of the specimens significantly improve. The area of the hysteresis loop gradually increases with the longitudinal reinforcement ratio, enhancing the energy dissipation capacity and improving the seismic performance of the UHPC columns. Therefore, increasing the longitudinal reinforcement ratio in UHPC columns can enhance their seismic resistance and elevate the ultimate load-carrying capacity of the members.

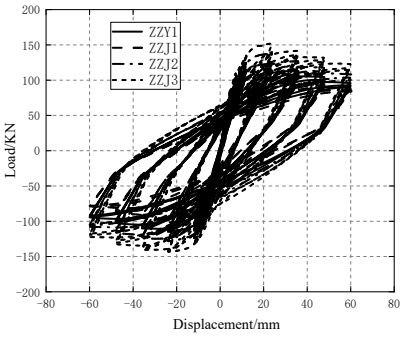

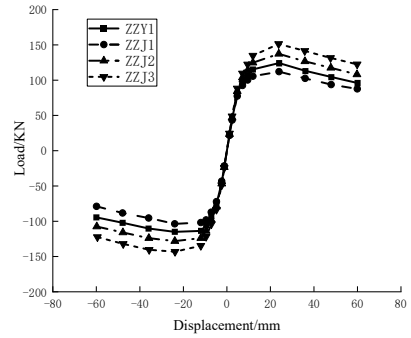

Hysteresis Curve Comparison Skeleton Curve Comparison

Fig. 8 Comparison of Longitudinal Reinforcement Ratios of UHPC Columns

4.3. Stirrup Spacing

Fig. 9 shows the skeleton curves and hysteresis curves of UHPC columns with different stirrup spacings, where the stirrup spacings are 60mm, 80mm,100 mm, and120 mm, respectively. Analysis indicates that prior to reaching peak load, the hysteresis curves and skeleton curves for different stirrup spacings exhibit essentially identical shapes. This demonstrates that stirrup spacing has minimal influence on peak load. Beyond peak load, specimens with smaller stirrup spacings display a more gradual decline in the skeleton curve's descending segment, indicating slower stiffness degradation and a reduced slope during the decline phase. The differences in the slope of the descending segment of the skeleton curves for UHPC column specimens with different stirrup spacings are not significant. Therefore, increasing the stirrup spacing is feasible in practical engineering applications.

ISSN: 2710-0588

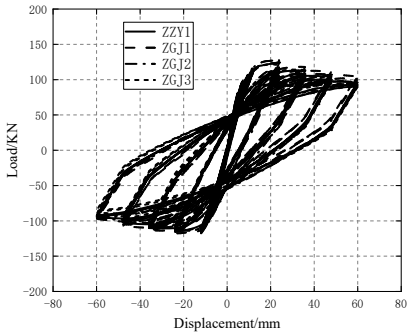

Hysteresis Curve Comparison

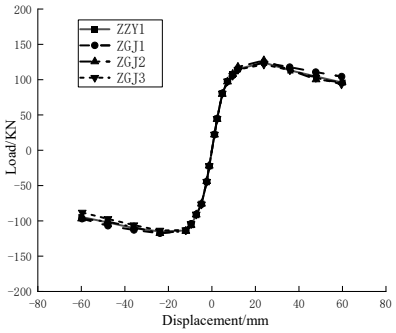

Skeleton Curve Comparison

Fig. 9 Comparison of UHPC Column Hoop Spacing

5. Conclusion

The CDP parameters derived from Sidoroff's energy equivalence principle and the selected UHPC stress-strain relationship are applicable to UHPC materials. When applied to numerical simulations of UHPC columns, they yield satisfactory results with minimal deviation from experimental data. ABAQUS finite element analysis can be effectively utilized for investigating the seismic performance of UHPC columns. As the axial compression ratio increases, the load-bearing capacity of UHPC columns rises while ductility decreases, eventually exhibiting significant brittleness at a certain threshold. Increasing the longitudinal reinforcement ratio markedly enhances the ultimate load-bearing capacity of UHPC columns. While increasing the stirrup spacing does not substantially boost the load-bearing capacity of UHPC columns, it is feasible to increase the stirrup spacing in engineering applications to ensure safety and reliability.

References

[1] YU R, SPIESZ P, BROUWERS H J H. Mix design and properties assessment of Ultra-High Performance Fibre Reinforced Concrete (UHPFRC) [J]. Cement and Concrete Research, 2014, 56: 29-39.

[2] SHI C,WU Z,XIAO J, et al. A review on ultra high performance concrete: Part I. Raw materials and mixture design [J]. Construction and Building Materials, 2015, 101: 741-751.

[3] Krahl P A, Gidrão G D M S, Carrazedo R. Compressive behavior of UHPFRC under quasi-static and seismic strain rates considering the effect of fiber content [J]. Construction and Building Materials, 2018, 188: 633-644.

[4] Zhu Yinglei. Research on Properties and Applications of Active Powder Concrete [J]. Concrete,2000,(07):31-34.

[5] Ma Fudong, Deng Mingke, Yang Yong. Seismic Performance of Prefabricated Frame Beam-Column Joints in Ultra-High Performance Concrete [J]. Engineering Mechanics,2021,38(10):90-102.

[6] Ju Yanzhong; Wang Dehong; Bai Junfeng. Experimental Study on Seismic Performance of Active Powder Concrete Columns [J]. Journal of Harbin Institute of Technology,2013,45(08):111-116.

[7] Ju Yanzhong; Li Chunyu; Wang Dehong. Nonlinear finite element analysis of seismic performance of beam-column joints in reactive powder concrete (RPC) structures [J]. Journal of Applied Basic and Engineering Sciences,2015,23(05):932-941.

[8] Zhao Guanyuan, Yan Guiping. Experimental Study on Seismic Performance of Active Powder Concrete Columns [J]. Journal of China Safety Science,2004,(07):97-100.

[9] Pan Jin. Experimental Study on Seismic Performance of Ultra-High Performance Concrete Columns with High-Strength Reinforcing Bars [D]. Hebei University of Technology,2023.

ISSN: 2710-0588

[10] Yang Zhihui. Study on Tensile Mechanical Properties of Active Powder Concrete with Different Steel Fiber Dosages [D]. Beijing Jiaotong University,2006.

[11] Sun Qingzhao. Overview of ABAQUS Plastic Damage Models for Concrete [J]. Chongqing Architecture,2014,13(11):70-72.

[12] Sidoroff F Description of anisotropic damage application to elasticity[M]. Berlin:Heideberg, 1981:237-244.

[13] Fang Zihu, Zhen Yi, Li Xiangpeng. Hysteretic Model of Reinforced Concrete Structures [J]. Journal of Wuhan University (Engineering Science),2018,51(07):613-619.